Journal of Materials Chemistry A

RSC Publishing

PAPER

View Article Online
View Journal | View Issue

Conjugated polymers consisting of quinacridone and quinoxaline as donor materials for organic photovoltaics: orientation and charge transfer properties of polymers formed by phenyl structures with a quinoxaline derivative†

Cite this: *J. Mater. Chem. A*, 2013, **1**, 6010

Ho-Jun Song, Doo-Hun Kim, Eui-Jin Lee and Doo-Kyung Moon*

Received 3rd February 2013
Accepted 18th March 2013

DOI: 10.1039/c3ta10512a

www.rsc.org/MaterialsA

In this study, a highly soluble poly[quinacridone-*alt*-quinoxaline] series (PQCQx, PQCTQx, PQCTPz) was synthesized through the Suzuki coupling reaction by introducing planar quinacridone and highly soluble quinoxaline. The polymers were soluble in general organic solvents, and the M_n was 15.6–85.0 kg mol^{-1}. The optical band gap energy was 1.82–1.97 eV, which was similar to the band gap of a benzothiadiazole derivative. The HOMO and LUMO levels of the polymers were −5.32 to −5.46 eV and −3.40 to 3.50 eV, respectively. According to XRD measurements, the PQCQx and PQCTPz showed the formation of an ordered lamellar structure and conventional edge-on π-stacking, while the PQCTQx showed face-on formation relative to the substrate. This study also evaluated the OPV characteristics by fabricating a bulk-heterojunction-type polymer solar cell. For the device structure of ITO/PEDOT:PSS/active layer (PQCTQx:$PC_{71}BM$ = 1 : 2 with DIO)/PFN/Al, the values of open-circuit voltage (V_{OC}), short-circuit current (J_{SC}), fill factor (FF) and power conversion efficiency (PCE) were 0.85 V, 7.6 mA cm^{-2}, 54.9%, and 3.6%, respectively.

Introduction

Semiconducting polymers have been used in diverse applications, such as in organic light emitting diodes (OLEDs),[1–4] organic photovoltaic cells (OPVs),[5–11] and organic thin film transistors (OTFTs),[12,13] for several decades. Among these applications, OPVs have drawn significant attention due to the global technology trend toward economic feasibility and continuous development coupled with preservation of the environment. However, the low power conversion efficiency (PCE) of these materials has been the greatest obstacle in developing OPVs.[6] The donor–acceptor (D–A) type low-band gap polymer has drawn much attention in recent years because its electronic properties can easily be changed based on the unique combination of the D–A unit. This polymer can also increase absorption at long wavelengths.[6] Nevertheless, the low power conversion efficiency (PCE) has remained the largest obstacle in D–A-type polymers.

The following idealistic conditions are required in D–A-type polymers to improve the PCE:[14] (1) a low band gap with a wide absorption area, (2) ordered orientation to produce good charge transport characteristics, (3) a low highest occupied molecular orbital (HOMO) energy level with which to produce a high open-circuit voltage (V_{oc}) and (4) an appropriate lowest unoccupied molecular orbital (LUMO) energy level for effective electron charge transfer to fullerene.

To acquire good charge transport characteristics, it is necessary to increase the close packing between polymers through the reduction of energetic disorder by increasing the coplanarity and interchain π–π interaction. Quinacridone (QC) derivatives are appropriate candidates for this process. QC derivatives, which are known as red-violet pigments, have an ordered structure and self-assembled characteristics, so they have drawn significant attention for use in OTFTs because of their high mobility.[15,16] The Takimiya group has recently reported a polymer composed of QC derivatives with a high hole mobility (0.2 cm^2 V^{-1} s^{-1}) for use in OTFTs.[17] We have synthesized PQCDTB by introducing a QC derivative as a donor and reported the properties of its self-organization.[18] However, the QC derivative has a low solubility due to its rigid structure. Thus, a derivative with a high solubility must be introduced when a polymer is synthesized with a QC derivative.

Among the D–A polymer's acceptor units, quinoxaline derivatives have been the most widely used due to the electron withdrawing properties of the two imine nitrogen atoms. Quinoxaline derivatives can be easily structurally deformed

Department of Material Chemistry and Engineering, Konkuk University, Seoul, 143-701, Korea. E-mail: dkmoon@konkuk.ac.kr; Fax: +82 822 444 0765; Tel: +82 822 450 3498

† Electronic supplementary information (ESI) available. See DOI: 10.1039/c3ta10512a

because of their high solubility, and their electronic properties can be changed with various substituents.[19,20] Therefore, if a QC derivative with a low solubility is introduced as a donor and a quinoxaline derivative with a high solubility is introduced as an acceptor, the synthesized polymer will exhibit outstanding solubility and the unique properties of both QC and quinoxaline.

In this study, we synthesized three D–A-type polymers by introducing QC and quinoxaline derivatives. It was expected that the synthesized polymers would show effective self-organization and a strong intra-molecular charge transfer property.

Results and discussion

Scheme 1 reveals the chemical structure of both the monomer and the polymer and their synthetic processes. As shown in Scheme 1, all polymers were synthesized through the Suzuki coupling reaction using **M1**, **M2**, **M3**, and **M4** and included poly(quinacridone-quinoxaline) (PQCQx), poly(quinacridone-diphenylquinoxaline) (PQCTQx), and poly(quinacridone-dibenzophenazine) (PQCTPz). The polymerization was carried out at 90 °C for 24 hours with a palladium(0) catalyst, 2 M potassium

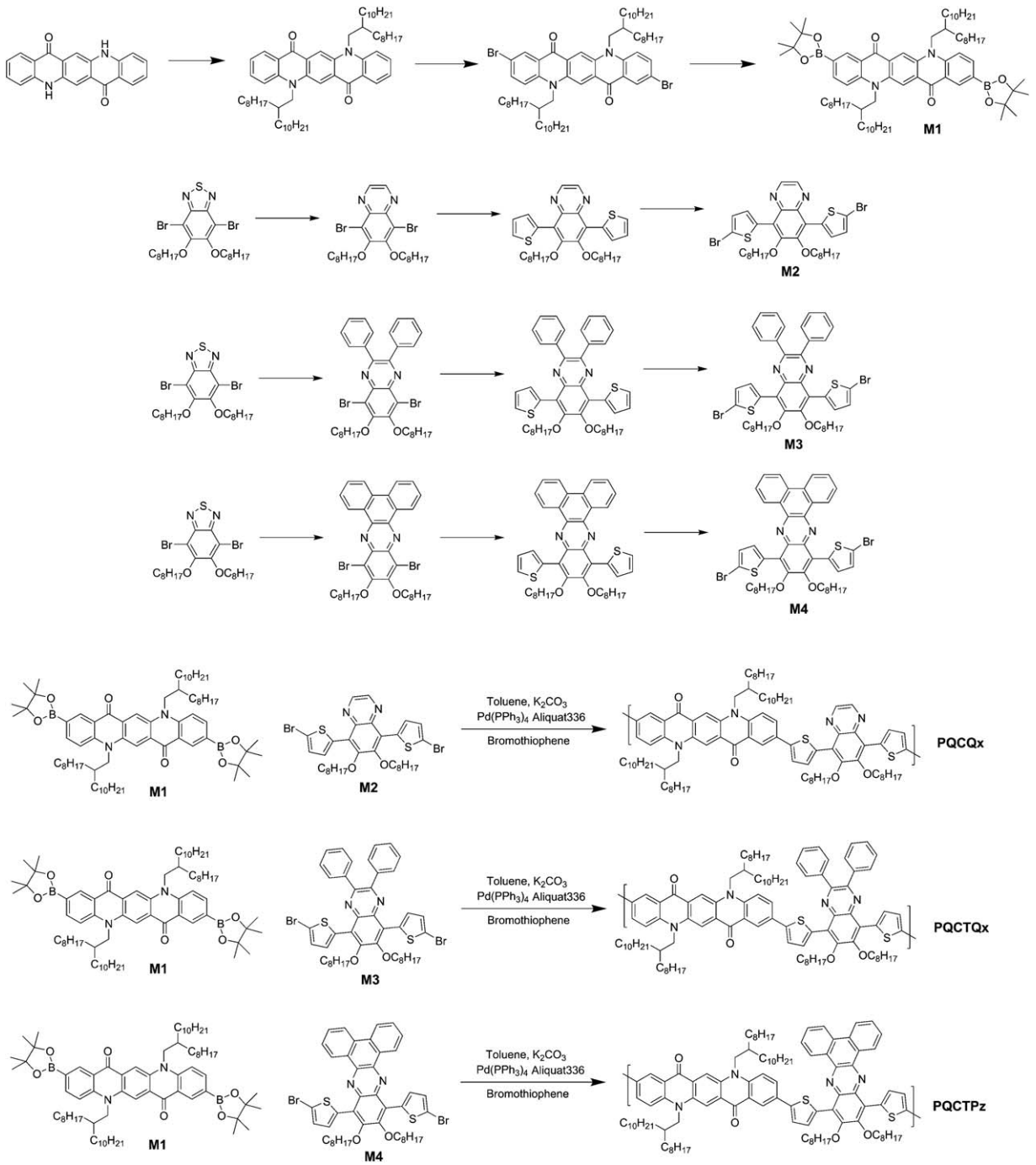

Scheme 1 Scheme of monomer synthesis and polymerization.

carbonate solution, Aliquat 336 as a surfactant, and toluene as the solvent. After the polymerization concluded, the polymer was end-capped with bromothiophene. The synthesized polymer was purified by Soxhlet extraction with solvents in the order of methanol, acetone, and chloroform. The polymer was then recovered from the chloroform fraction and precipitated into methanol. As a result, the yields of PQCQx, PQCTQx, and PQCTPz reached 55, 73, and 72%, respectively. The obtained polymer was soluble in organic solvents such as THF, chloroform, chlorobenzene, and *o*-dichlorobenzene. A homogeneous semitransparent film of red or violet was formed through spin-coating.

Table 1 shows the molecular weight and thermal properties of the polymers. When GPC analyses were made using polystyrene as the standard, the number-average molecular weights (M_n) of the PQCQx, PQCTQx, and PQCTPz were 15.6, 85.0, and 44.2 kg mol^{-1}, respectively. In contrast, the polydispersity indices (PDIs) showed a distribution of 2.60, 7.17, and 2.14, respectively. The degree of polymerization in PQCTQx was higher than that in PQCTPz because dibenzophenazine has a rigid structure and polymerization becomes less effective with a rigid backbone structure.[6] Table 1 shows the results of the thermal analysis performed by TGA. PQCQx, PQCTQx, and PQCTPz experienced a 5% weight loss at temperatures of 327, 347, and 328 °C, respectively, indicating high thermal stability due to the rigid QC structure. This stability makes the polymers applicable to optoelectronic devices and OPVs, both of which require a thermal stability at temperatures of 300 °C or greater.[18] In particular, the degradation temperature of PQCTQx was 20 °C higher than that of PQCQx and PQCTPz, which may be due to its degree of polymerization. We investigated the thermal behavior using DSC analysis (see ESI†), which revealed no obvious thermal transitions in any of the polymers within the temperature range of 40 to 250 °C.

Fig. 1 shows the UV-visible spectra of the polymers. The maximum absorption peaks of PQCQx (λ_{max}) were observed at 370 nm and 440 nm in solution (10^{-6} M, in chloroform). In contrast, the maximum absorption peaks of PQCTQx and PQCTPz (λ_{max}) were observed at 388 and 537 nm and 400 and 548 nm in solution, respectively. The band at approximately 350–400 nm in the absorption spectra of the polymers was assigned to the π–π* transition, whereas the 530–600 nm band occurred due to intramolecular charge transfer (ICT) between the donor and the acceptor moieties.[10] The absorption spectrum of PQCTPz was broadened and redshifted compared with that of PQCQx and PQCTQx, which can be explained by the ICT effects that are much stronger in PQCTPz than in PQCQx and PQCTQx due to the phenyl ring structure. The maximum absorption

Table 1 Molecular weight and thermal properties of the polymers

Polymers	M_n (kg mol^{-1})	M_w (kg mol^{-1})	PDI	T_d[a]
PQCQx	15.6	40.9	2.60	327
PQCTQx	85.0	610.6	7.17	347
PQCTPz	44.2	94.9	2.14	328

[a] Temperature resulting in 5% weight loss based on the initial weight.

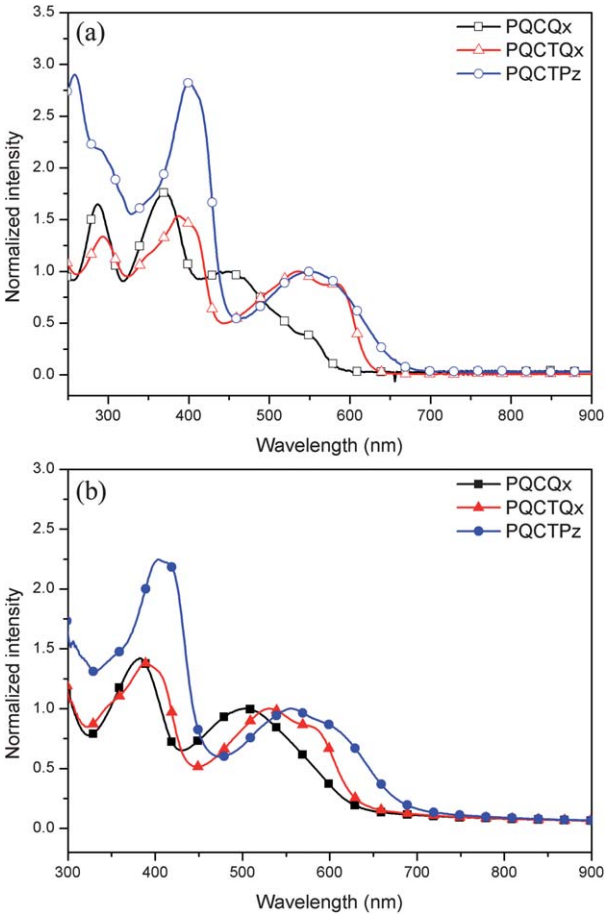

Fig. 1 Absorption spectra of polymers in solution (10^{-6} M) and film (50 nm).

spectra of the polymers in the film were redshifted by 1–57 nm compared with those in the solution. These results were explained by their much more planar conformations in the solid state. The calculated optical band gaps of PQCQx, PQCTQx, and PQCTPz through the UV onset value of the film were 1.97, 1.96, and 1.82 eV, respectively.

Fig. 2 shows the cyclic voltammograms of PCZDTB and PQCDTB, which were measured in 0.1 M tetrabutyl ammonium-

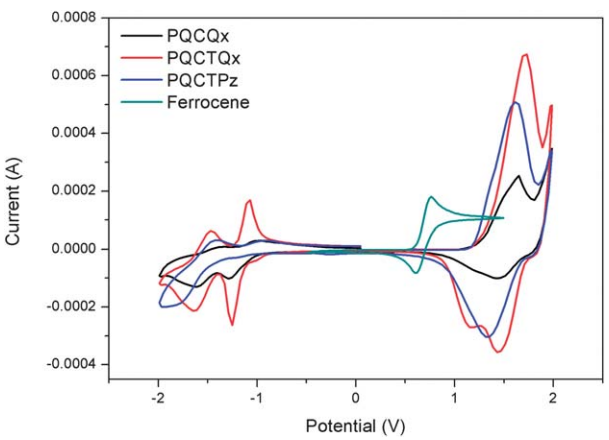

Fig. 2 Cyclic voltammograms of polymers with a 0.1 M acetonitrile (substituted with nitrogen for 5 min) solution.

Table 2 Optical and electrochemical properties of the polymers

Polymer	Absorption, λ_{max} (nm)		E_{ox}^{onset} (V)	E_{HOMO}[c] (eV)	E_{LUMO}[d] (eV)	E_{opt}[e] (eV)
	Solution[a]	Film[b]				
PQCQx	287, 370, 448	382, 505	1.25	−5.37	−3.40	1.97
PQCTQx	293, 388, 537	389, 531	1.34	−5.46	−3.50	1.96
PQCTPz	358, 400, 548	404, 555	1.20	−5.32	−3.50	1.82

[a] Absorption spectrum in $CHCl_3$ solution (10^{-6} M). [b] Spin-coated thin film (50 nm). [c] Calculated from the oxidation onset potentials under the assumption that the absolute energy level of Fc/Fc^+ was −4.8 eV relative to the vacuum level. [d] HOMO − E_{opt}. [e] Estimated from the onset of UV-vis absorption data of the thin film.

hexafluorophosphate acetonitrile. Unlike the PQA2T (poly[quinacridone-bithiophene]) reported by Takimiya *et al.*, a clear oxidation-reduction peak was observed in all of the polymers.[17] This type of result was obtained because the polymers were D–A structured, unlike the typical p-type structure of PQA2T. The oxidation onset potentials (E_{ox}^{onset}) of the PQCQx, PQCTQx, and PQCTPz were +1.25, 1.34, and 1.20 V, and the HOMO levels achieved through calculation were −5.37, −5.46, and −5.32 eV, respectively. The optical and electrochemical properties of the polymers are summarized in Table 2. The HOMO levels of the polymers (between −5.32 and −5.46 eV) were 0.1–0.2 eV lower than those reported for PQCDTB (−5.24 eV) with a benzothiadiazole derivative due to the quinoxaline derivative.[21,22] Because the HOMO levels of PQCQx, PQCTQx, and PQCTPz are lower than those of PQCDTB,[18] a relatively high air stability and open circuit voltage (V_{OC}) were obtained. The LUMO energy levels were calculated from the difference between the HOMO energy levels and the optical band gap energies. According to these calculations, the LUMO levels of PQCQx, PQCTQx, and PQCTPz were −3.40, −3.50, and 3.50 eV, respectively.

Fig. 3 shows the band diagram of the energy levels obtained through CV measurements and the HOMO and LUMO distributions obtained using density functional theory (DFT) calculations in Gaussian at the B3LYP/6-31G* level. As shown in Fig. 3, the LUMO level of PQCTQx and PQCTPz (−3.50 eV) was lower than that of PQCQx (−3.40 eV) by 0.1 eV. Therefore, if charge separation occurred after receiving light energy, an electron in PQCTQx and PQCTPz would exhibit more effective charge transport to PCBM than an electron in PQCQx in the active layer.[14]

As shown in the HOMO and LUMO distributions of the polymers, the LUMO orbitals of PQCQx and PQCTQx were

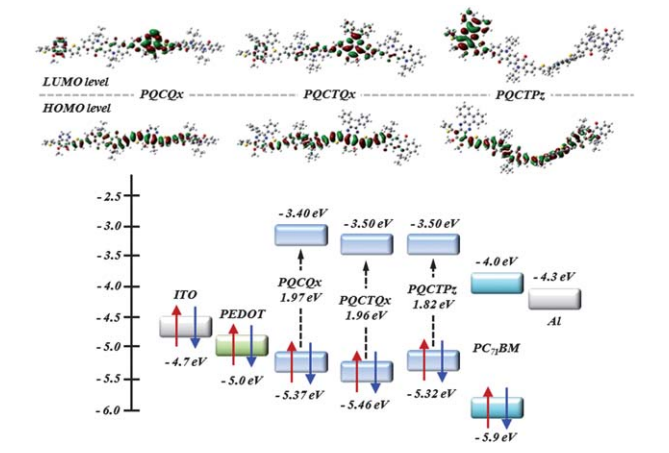

Fig. 3 DFT Gaussian simulation and band diagram of polymers (experiment level), ITO, $PC_{71}BM$, Al.

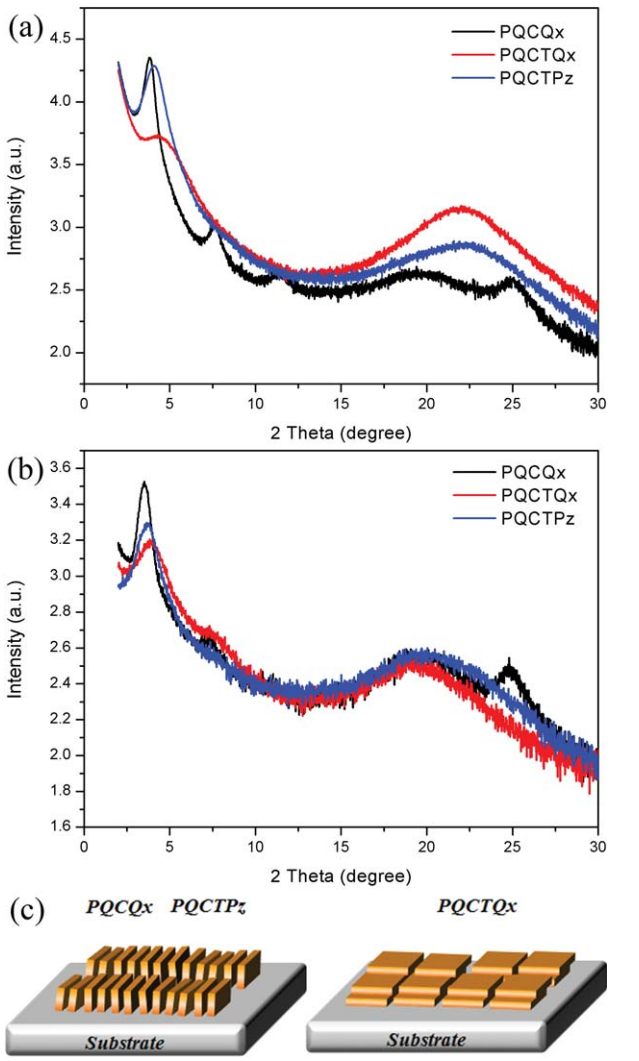

Fig. 4 (a) Out-of-plane and (b) in-plane X-ray diffraction patterns of thin films after thermal treatment. (c) Schematic representation of interdigitated packing structure.

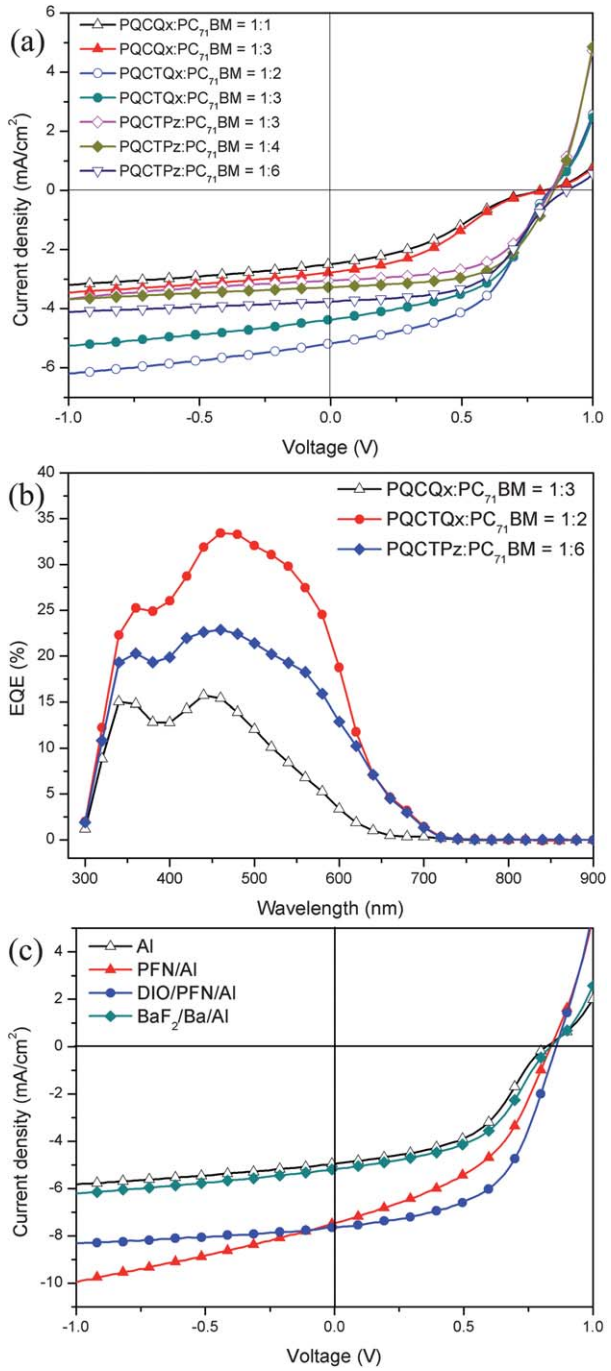

Fig. 5 (a) *J–V* characteristics, (b) EQE spectra and (c) *J–V* characteristics with PFN of the BHJ solar cells.

partially located on the donor QC derivative, which suggested an incomplete ICT effect. In contrast, the LUMO orbitals of PQCTPz were located mostly on the acceptor quinoxaline derivative, which suggested a strong ICT effect.[23] This result was confirmed by the aforementioned UV-vis results (Fig. 1).

Fig. 4 shows X-ray diffraction measurements of the film used to analyze the ordering structure of the obtained polymers. As shown in Fig. 4(a), sharp diffraction peaks were observed at 3.8 and 4.0° in the out-of-plane peak of PQCQx and PQCTPz, respectively, which indicated the formation of an ordered lamellar structure as an out-of-plane peak (100) by the alkyl side chain of quinacridone and conventional edge-on π-stacking.[17,18] The lamellar *d*-spacings (d_1) of PQCQx and PQCTPz were 23.2 and 22.0 Å ($\lambda = 2d\sin\theta$), respectively. Broad diffraction peaks were detected at approximately 24.8 and 19.7° in the (010) in-plane patterns of PQCQx and PQCTPz related to π–π stacking, as shown in Fig. 4(b). Using the same calculation, the π–π stacking distances (d_π) of PQCQx and PQCTPz were 3.6 and 4.5 Å, respectively. The results for PQCQx were similar to those of thiophene and thiophene-fused aromatic system polymers that perform well as OPVs.[17,24] In contrast, the results for PQCTPz were similar to the results for the π–π stacking (d_π = 4.0–4.4 Å) of fluorene–thiophene. Interestingly, a weak (100) diffraction peak with a *d*-spacing of 20.5 Å was observed in PQCTQx, whereas the (010) diffraction corresponding to π–π stacking with a *d*-spacing of 4.0 Å was more prominent. This result suggested that a large fraction of the PQCTQx backbones were oriented face-on relative to the substrate. In other words, the π-stacking direction was perpendicular to that of the substrate.[5] This difference in the π-stacking orientation relative to the substrate could have arisen from the difference in the shape of the phenyl structure with the quinoxaline derivative.[5]

The tilt angles were comparatively analyzed by calculating the PQCQx, PQCTQx, and PQCTPz configurations using a DFT calculation. The tilt angles between thiophene and quinacridone were 19–21° in PQCQx and PQCTQx and 23–25° in PQCTPz. The formation of a planar backbone was observed in PQCQx and PQCTQx, but not in PQCTPz (see ESI†). Based on this result, it was confirmed that π–π stacking was more effective in PQCQx and PQCTQx than in PQCTPz due to the steric hindrance of the phenazine unit (fused phenyl structure) that was introduced to the main chain of PQCTPz.[13]

Fig. 5 and Table 3 show the results of an evaluation of OPV device characteristics. The devices were structured as follows: ITO (170 nm)/PEDOT:PSS (40 nm)/active layer (50 nm)/BaF_2 (2 nm)/Ba (2 nm)/Al (100 nm). The active layer had an optimized blending ratio obtained by dissolving the polymer and phenyl-C71-butyric acid methyl ester ($PC_{71}BM$) in *o*-dichlorobenzene (*o*-DCB) at a concentration of approximately 0.5–1 wt%. We fabricated more than 200 devices to confirm reproducibility. The open-circuit voltage (V_{OC}), short-circuit current (J_{SC}), fill factor (FF), and power conversion efficiency (PCE) were 0.83 V, 5.3 mA cm^{-2}, 51.1% and 2.3%, respectively, for PQCTQx at a ratio of 1 : 2 with $PC_{71}BM$ (50 nm thick). The PQCTQx device

Table 3 Photovoltaic performance of the BHJ solar cells.

Active layer (w/w)						
Polymer (P)	Acceptor (A)	Weight ratio (P : A, w/w)	V_{OC} (V)	J_{SC} (mA cm^{-2})	FF (%)	PCE (%)
PQCQx	$PC_{71}BM$	1 : 1	0.81	2.5	32.6	0.6
		1 : 3	0.81	2.8	33.7	0.7
PQCTQx	$PC_{71}BM$	1 : 2	0.83	5.3	51.1	2.3
		1 : 3	0.83	4.4	51.0	1.9
PQCTPz	$PC_{71}BM$	1 : 3	0.83	3.0	56.5	1.4
		1 : 4	0.85	3.3	58.0	1.6
		1 : 6	0.89	3.8	51.8	1.8

showed the best performance, with a high photo-current that occurred due to the high molecular weight and face-on orientation compared with PQCQx and PQCTPz.[5,25] In contrast, the efficiency of the PQCTPz device tended to improve with increasing $PC_{71}BM$. At a PQCTPz to $PC_{71}BM$ ratio of 1 : 6, the values of V_{OC}, J_{SC}, FF, and PCE were 0.89 V, 3.8 mA cm^{-2}, 51.8%, and 1.8%, respectively. Though the PQCTPz device had a broader absorption than the PQCTQx device due to a strong

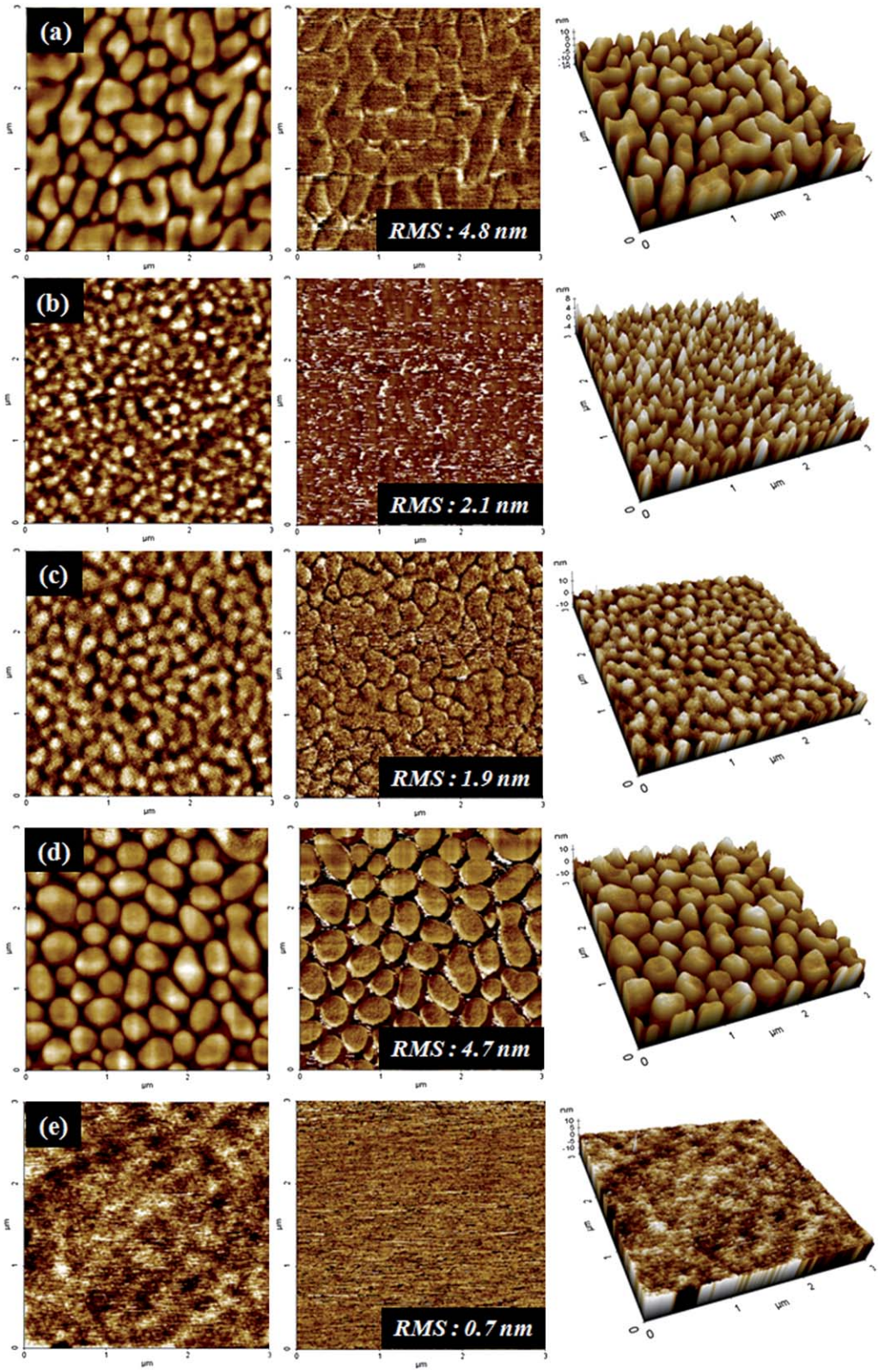

Fig. 6 Topographic AFM images of (a) PQCQx:$PC_{71}BM$ 1 : 3, (b) PQCTQx:$PC_{71}BM$ 1 : 2, (c) PQCTQx:$PC_{71}BM$ 1 : 3, (d) PQCTPz:$PC_{71}BM$ 1 : 3 and (e) PQCTPz:$PC_{71}BM$ 1 : 6.

intramolecular charge transfer property, it had a lower level of performance than the PQCTQx device. This result suggested that the molecular weight and orientation affected the PCE value more than the intramolecular charge transfer. The PQCQx device had the lowest level of performance, with low J_{SC} (2.8 mA cm^{-2}) and FF values (33.7%), which were due to its low molecular weight and the morphology of the macro phase separation, as shown in Fig. 6(a). The V_{oc} of the polymers containing the quinoxaline derivative was somewhat greater than that of the reported PQCDTB with a benzothiadiazole derivative ($V_{oc} = 0.79$ V).[18] This result was obtained because the polymers had lower HOMO levels (between −5.32 and −5.46 eV) than PQCDTB (−5.24 eV).

To check the accuracy of the device measurements their external quantum efficiency (EQE) was measured. The EQE curve for various ratios of $PC_{71}BM$ are shown in Fig. 5(b). The photons in the EQE curve occurred mostly in the polymer phase, which correlated with the absorption spectra of the polymers.[26] The EQE curve was similar to the UV-vis spectra curve in Fig. 1. The short-circuit current density of PQCTQx obtained from the EQE compared with that of $PC_{71}BM$ (1 : 2 ratio) was 5.0 mA cm^{-2}, while the theoretical short-circuit current density of PQCTPz obtained from the EQE compared with that of $PC_{71}BM$ (1 : 6 ratio) was 3.0 mA cm^{-2}. The EQE of PQCTQx led to a larger current density than that of PQCTPz because of the high molecular weight of PQCTQx (85.0 kg mol^{-1}) compared with that of PQCTPz (44.2 kg mol^{-1}).[25]

Recently, a number of studies have been aimed at improving the performance of devices using poly [(9,9-bis(30-(*N*,*N*-dimethylamino)propyl)-2,7-fluorene)-*alt*-2,7-(9,9-dioctylfluorene)] (PFN) because PFN improves the interfacial adhesion and electron transport between active layers and cathodes.[27] Thus, we fabricated the devices introducing PFN for 1 : 2 PQCTQx/$PC_{71}BM$ ratio and the results are summarized in Fig. 5(c) and Table 4. For the device structure of ITO/PEDOT:PSS/active layer (PQCTQx:$PC_{71}BM$ = 1 : 2)/Al, the values of V_{OC}, J_{SC}, FF, and PCE were 0.81 V, 4.9 mA cm^{-2}, 49.0%, and 2.0%, respectively. On the other hand, for the device structure of ITO/PEDOT:PSS/active layer (PQCTQx:$PC_{71}BM$ = 1 : 2 with DIO)/PFN/Al, the values of V_{OC}, J_{SC}, FF, and PCE were 0.85 V, 7.6 mA cm^{-2}, 54.9%, and 3.6%, respectively. The device with PFN showed the best performance with improved J_{SC} and FF compared with the device without PFN because the PFN interlayer improved the electron transport property between active layers and Al.

Atomic force microscopy (AFM) was used to investigate the morphology of the polymer/PCBM blend film, and the result is shown in Fig. 6. Micro-phase separation occurred between the PQCTQx and $PC_{71}BM$, as shown in Fig. 6(b), while the PQCTQx formed a small size domain at a 1 : 2 PQCTQx/$PC_{71}BM$ ratio. In contrast, when the PQCQx/$PC_{71}BM$ ratio was 1 : 3, PQCQx assembled as shown in Fig. 6(a), and a large domain with a length of 1 μm was formed. A relatively large phase separation occurred as a result. Similarly, the PQCTPz formed a large domain with a length of 0.5 μm at a 1 : 3 PQCTPz/$PC_{71}BM$ ratio, as shown in Fig. 6(d). The large phase separation exhibited a low photocurrent by reducing the charge separation and increasing the exciton diffusion length and recombination of electric charges.[28] Therefore, a large phase separation occurred between the polymer and the $PC_{71}BM$ in the PQCQx/$PC_{71}BM$ and PQCTPz/$PC_{71}BM$ blends. A low photocurrent occurred as a result, which was comparable to that of the PQCTQx/$PC_{71}BM$ blend. The same results were confirmed for the current device using the data in Table 3. A uniquely smooth morphology was detected at a 1 : 6 PQCTPz/$PC_{71}BM$ ratio, which showed the highest photo-current density of all the PQCTPz/$PC_{71}BM$ blend ratios.

Table 4 Photovoltaic performance of the various device structures

Device structure	V_{OC} (V)	J_{SC} (mA cm^{-2})	FF (%)	PCE (%)
PQCTQx:$PC_{71}BM$/Al	0.81	4.9	49.0	2.0
PQCTQx:$PC_{71}BM$/PFN/Al	0.83	7.4	45.0	2.8
PQCTQx:$PC_{71}BM$/PFN/Al[a]	0.85	7.6	54.9	3.6
PQCTQx:$PC_{71}BM$/BaF_2/Ba/Al	0.83	5.3	51.1	2.3

[a] DIO of 3 vol% in the active layer.

Experiment section

Instruments and characterization

Unless otherwise specified, all the reactions were carried out under a nitrogen atmosphere. Solvents were dried by standard procedures. All column chromatography procedures were performed with the use of silica gel (230–400 mesh, Merck) as the stationary phase. ^{1}H NMR spectra were measured on a Bruker ARX 400 spectrometer using solutions in $CDCl_3$ and chemical shifts were recorded in ppm units with TMS as the internal standard. The elemental analyses were carried out using an EA1112 (CE Instruments). Electronic absorption spectra were measured in chloroform using a HP Agilent 8453 UV-vis spectrophotometer. The cyclic voltammetric waves were produced using a Zahner IM6eX electrochemical workstation with a 0.1 M acetonitrile (substituted with nitrogen for 20 min) solution containing tetrabutyl ammonium hexafluorophosphate (Bu_4NPF_6) as the electrolyte at a constant scan rate of 50 mV s^{-1}. ITO, a Pt wire, and silver/silver chloride [Ag in 0.1 M KCl] were used as the working, counter, and reference electrodes, respectively. The electrochemical potential was calibrated against Fc/Fc^+. The HOMO levels of the polymers were determined using the oxidation onset value. Onset potentials are values obtained from the intersection of the two tangents drawn at the rising current and the baseline changing current of the CV curves. TGA measurements were performed on a NETZSCH TG 209 F3 thermogravimetric analyzer. All GPC analyses were made using THF as an eluent and polystyrene standard as a reference. X-ray diffraction (XRD) patterns were obtained using SmartLab 3 kW (40 kV, 30 mA, Cu target, wavelength: 1.541871 ang), Rigaku, Japan. Topographic images of the active layers were obtained by atomic force microscopy (AFM) in tapping mode under ambient conditions using a XE-100 instrument. Theoretical study was performed by using density functional theory (DFT), as approximated by the B3LYP functional and employing the 6-31G* basis set in Gaussian 09.

Fabrication and characterization of polymer solar cells

All of the bulk-heterojunction PV cells were prepared using the following device fabrication procedure. The glass/indium tin oxide (ITO) substrates [Sanyo, Japan (10 Ω/γ)] were sequentially lithographically patterned, cleaned with detergent, and ultrasonicated in deionized water, acetone, and isopropyl alcohol. Then the substrates were dried on a hot-plate at 120 °C for 10 min and treated with oxygen plasma for 10 min in order to improve the contact angle just before the film coating process. Poly(3,4-ethylene-dioxythiophene):poly(styrene-sulfonate) (PEDOT:PSS, Baytron P 4083 Bayer AG) was passed through a 0.45 μm filter before being deposited onto ITO at a thickness of *ca.* 32 nm by spin-coating at 4000 rpm in air and then it was dried at 120 °C for 20 min inside a glove box. Composite solutions of polymers and PCBM were prepared using 1,2-dichlorobenzene (DCB). The concentration was controlled adequately in the 0.5 wt% range, and the solutions were then filtered through a 0.45 μm PTFE filter and then spin-coated (500–2000 rpm, 30 s) on top of the PEDOT:PSS layer. The PFN solution in methanol and acetic acid was spin-coated on top of the obtained active layer at 4000 rpm for 30 s to form a thin interlayer of 5 nm. The device fabrication was completed by depositing thin layers of BaF_2 (1 nm), Ba (2 nm), and Al (200 nm) at pressures of less than 10^{-6} torr. The active area of the device was 4.0 mm^2. Finally, the cell was encapsulated using UV-curing glue (Nagase, Japan).

The illumination intensity was calibrated using a standard Si photodiode detector that was equipped with a KG-5 filter. The output photocurrent was adjusted to match the photocurrent of the Si reference cell in order to obtain a power density of 100 mW cm^{-2}. After the encapsulation, all of the devices were operated under an ambient atmosphere at 25 °C. The current–voltage (*I–V*) curves of the photovoltaic devices were measured using a computer-controlled Keithley 2400 source measurement unit (SMU) that was equipped with a Peccell solar simulator under an illumination of AM 1.5G (100 mW cm^{-2}). Thicknesses of the thin films were measured using a KLA Tencor Alpha-step 500 surface profilometer with an accuracy of 1 nm.

5,8-Dibromo-6,7-bis(octyloxy) quinoxaline

Under a nitrogen atmosphere, 4,7-dibromo-5,6-bis(octyloxy)-benzo[*c*][1,2,5]thiadiazole (0.88 g, 1.59 mmol) and zinc (1.04 g, 15.9 mmol) dust were dissolved in 30 ml of acetic acid. The mixture was refluxed for 3 hours at 80 °C. After cooling to room temperature, the reaction mixture was washed with a NaOH solution. The solids that resulted after the evaporation of the organic solvent and oxalaldehyde (0.92 g, 15.92 mmol) were dissolved in 20 ml of acetic acid. The mixture was refluxed for 1 day at 60 °C. After cooling to room temperature, an orange colored mixture was observed. After filtration, the reaction mixture was purified by column chromatography on silica gel to obtain the product as a light yellow powder (0.54 g, 62.5%). ^{1}H NMR (400 MHz; $CDCl_3$; Me_4Si): 8.90(s, 2H; Ar) 4.20(t, 4H; CH_2) 1.93(m, 4H; CH_2) 1.55(m, 4H; CH_2) 1.33(m, 16H; CH_2) 0.89(t, 6H; CH_3) ^{13}C NMR (100 MHz; $CDCl_3$; Me_4Si): 154.23; 144.53; 139.44; 117.44; 74.96; 31.84; 30.30; 29.41; 29.28; 26.03; 22.67; 14.10. Anal. calcd for: $C_{24}H_{36}N_2O_2$: C, 52.95; H, 6.67; Br, 29.36; N, 5.15; O, 5.88 found: C, 53.02; H 6.69; N, 5.14; O, 6.67%.

6,7-Bis(octyloxy)-5,8-di(thiophen-2-yl)quinoxaline

5,8-Dibromo-6,7-bis(octyloxy)quinoxaline (1.14 g, 2.09 mmol) and tributyl(thiophen-2-yl)stannane (2.00 ml, 6.28 mmol) in toluene (55 ml) were added to $PdCl_2(PPh_3)_2$ (0.16 g, 0.23 mmol) under a nitrogen atmosphere. After refluxing for 24 hours at 120 °C, the mixture was cooled to room temperature and then poured into H_2O; the organic layer was extracted with $CHCl_3$ and dried over anhydrous Na_2SO_4. The crude product was purified by column chromatography on silica gel to obtain the product as a yellow oil (0.82 g, 71.2%). ^{1}H NMR (400 MHz; $CDCl_3$; Me_4Si): 8.90(s, 2H; Ar) 7.68(d, 2H; Ar) 7.54(d, 2H; Ar) 7.23(d, 2H; Ar) 4.00(t, 4H; CH_2) 1.73(m, 4H; CH_2) 1.36(m, 4H; CH_2) 1.29(m, 16H; CH_2) 0.92(t, 6H; CH_3). ^{13}C NMR (100 MHz; $CDCl_3$; Me_4Si): 153.25; 142.84; 139.65; 133.29; 130.65; 127.51; 126.39; 125.38; 74.31; 31.86; 30.31; 29.43; 29.28; 25.97; 22.71; 14.15.

5,8-Bis(5-bromothiophen-2-yl)-6,7-bis(octyloxy)quinoxaline (M2)

Under a nitrogen atmosphere, 6,7-bis(octyloxy)-5,8-di(thiophen-2-yl)quinoxaline (1.42 g, 2.58 mmol) was dissolved in 60 ml of chloroform and 60 ml of acetic acid, and then NBS (1.06 g, 5.93 mmol) was added in portions. The mixture was stirred for 24 h at room temperature. The mixture was then poured into water and extracted with chloroform. The combined organic layers were dried over Na_2SO_4, and the solvent was removed. The crude product was purified by column chromatography to obtain the product as a dark yellow oil (1.3 g, 70.1%). ^{1}H NMR (400 MHz; $CDCl_3$; Me_4Si): 8.63(s, 2H; Ar) 7.60(d, 2H; Ar) 7.01(d, 2H; Ar) 3.92(t, 4H; CH_2) 1.68(m, 4H; CH_2) 1.36(m, 4H; CH_2) 1.29(m, 16H; CH_2) 0.92(t, 6H; CH_3). ^{13}C NMR (100 MHz; $CDCl_3$; Me_4Si): 152.97; 142.36; 138.62; 134.86; 131.20; 127.08; 124.12; 115.87; 74.31; 31.90; 30.43; 29.77; 29.28; 26.08; 22.76; 14.20.

5,8-Dibromo-6,7-bis(octyloxy)-2,3-diphenylquinoxaline

Under a nitrogen atmosphere, 4,7-dibromo-5,6-bis(octyloxy)-benzo[*c*][1,2,5]thiadiazole (4.0 g, 7.27 mmol) and zinc (5.88 g, 90.0 mmol) dust were dissolved in 110 ml of acetic acid. The mixture was refluxed for 3 hours at 80 °C. After cooling to room temperature, the reaction mixture was washed with a NaOH solution. The solids that resulted after the evaporation of the organic solvent and benzil (3.36 g, 15.92 mmol) were dissolved in 110 ml of acetic acid. The mixture was refluxed for 1 day at 60 °C. After cooling to room temperature, an orange colored mixture was observed. After filtration, the reaction mixture was purified by column chromatography on silica gel (dichloromethane as an eluent) to obtain the product as a green solid (3.2 g, 63.4%). ^{1}H NMR (400 MHz; $CDCl_3$; Me_4Si): 7.62(d, 4H; Ar) 7.37(m, 6H; Ar) 4.20(t, 4H; CH_2) 1.92(m, 4H; CH_2) 1.55(m, 4H; CH_2) 1.33(m, 16H; CH_2) 0.90(t, 6H; CH_3) ^{13}C NMR (100 MHz; $CDCl_3$; Me_4Si): 153.81; 152.69; 138.24; 137.14; 130.22; 129.25; 128.30; 117.26; 74.86; 31.88; 30.33; 29.45; 29.31; 26.07; 22.70;

14.13. Anal. calcd for: $C_{36}H_{44}Br_2N_2O_2$: C, 62.07; H, 6.37; N, 4.02; O, 4.59 found: C, 61.20; H, 6.44; N, 3.92; O, 4.99%.

6,7-Bis(octyloxy)-5,8-di(thiophen-2-yl)-2,3-diphenylquinoxaline

5,8-Dibromo-6,7-bis(octyloxy)-2,3-diphenylquinoxaline (2.0 g, 2.87 mmol) and tributyl(thiophen-2-yl)stannane (2.73 ml, 8.61 mmol) in toluene (75 ml) were added to $PdCl_2(PPh_3)_2$ (0.203 g, 0.29 mmol) under a nitrogen atmosphere. After refluxing for 48 hours at 80 °C, the mixture was cooled to room temperature and then poured into H_2O; the organic layer was extracted with $CHCl_3$ and dried over anhydrous Na_2SO_4. The crude product was purified by column chromatography on silica gel to obtain the product as an orange solid (1.5 g, 74.3%). ^{1}H NMR (400 MHz; $CDCl_3$; Me_4Si): 8.05 (d, 2H; Ar) 7.65(d, 4H; Ar) 7.55(d, 2H; Ar) 7.33(m, 6H; Ar) 7.20(d, 2H; Ar) 4.03(t, 4H; CH_2) 1.77(m, 4H; CH_2) 1.39(m, 4H; CH_2) 1.29(m, 16H; CH_2) 0.90(t, 6H; CH_3). ^{13}C NMR (100 MHz; $CDCl_3$; Me_4Si): 152.88; 150.24; 138.93; 136.43; 133.49; 130.88; 130.32; 128.66; 128.14; 127.85; 126.06; 124.19; 74.10; 31.87; 30.41; 29.50; 29.31; 26.07; 22.71; 14.15. Anal. calcd for: $C_{44}H_{50}N_2O_2S_2$: C, 75.17; H, 7.17; N, 3.98; O, 4.55; S, 9.12 found: C, 73.14; H, 7.35; N, 3.83; O, 5.13; S, 7.85%.

5,8-Bis(5-bromothiophen-2-yl)-6,7-bis(octyloxy)-2,3-diphenylquinoxaline (M3)

Under a nitrogen atmosphere, 6,7-bis(octyloxy)-5,8-di(thiophen-2-yl)-2,3-diphenylquinoxaline (1.5 g, 2.13 mmol) was dissolved in 140 ml of THF, and then NBS (0.87 g, 4.9 mmol) was added in portions. The mixture was stirred for 24 h at room temperature. The mixture was then poured into water and extracted with chloroform. The combined organic layers were dried over Na_2SO_4, and the solvent was removed. The crude product was purified by column chromatography to obtain **M1** as an red-orange solid (1.2 g, 65.5%). ^{1}H NMR (400 MHz; $CDCl_3$; Me_4Si): 7.97(d, 2H; Ar) 7.63(d, 4H; Ar) 7.36(m, 6H; Ar) 7.14(d, 2H; Ar) 4.07(t, 4H; CH2) 1.83(m, 4H; CH2) 1.42(m, 4H; CH2) 1.30(m, 16H; CH2) 0.90(t, 6H; CH3). ^{13}C NMR (100 MHz; $CDCl_3$; Me_4Si): 152.68; 150.57; 138.46; 135.89; 135.19; 131.25; 130.33; 128.95; 128.89; 128.25; 123.35; 116.09; 74.22; 31.85; 30.42; 29.48; 29.30; 26.07; 22.70; 14.13. Anal. calcd for: $C_{44}H_{48}Br_2N_2O_2S_2$: C, 61.39; H, 5.62; N, 3.25; O, 3.72; S, 7.45 found: C, 61.23; H, 5.65; N, 3.13; O, 4.28; S, 7.42%.

10,13-Dibromo-11,12-bis(octyloxy)dibenzo[*a*,*c*]phenazine

Under a nitrogen atmosphere, 4,7-dibromo-5,6-bis(octyloxy)-benzo[*c*][1,2,5]thiadiazole (1.75 g, 3.18 mmol) and zinc (2.58 g, 39.4 mmol) dust were dissolved in 110 ml of acetic acid. The mixture was refluxed for 3 hours at 80 °C. After cooling to room temperature, the reaction mixture was washed with a NaOH solution. The solids that resulted after the evaporation of the organic solvent and 9,10-phenanthrenequinone (1.46 g, 7.0 mmol) were dissolved in 110 ml of acetic acid. The mixture was refluxed for 1 day at 60 °C. After cooling to room temperature, an orange colored mixture was observed. After filtration, the reaction mixture was purified by column chromatography on silica gel (dichloromethane as an eluent) to obtain the product as a light-yellow solid (1.3 g, 58.9%). ^{1}H NMR (400 MHz; $CDCl_3$; Me_4Si): 9.29 (d, 2H; Ar) 8.41 (t, 2H; Ar) 7.68 (m, 4H; Ar) 4.27(t, 4H; CH_2) 1.96(t, 4H; CH_2) 1.59(m, 4H; CH_2) 1.42(m, 16H; CH_2) 0.91(t, 6H; CH_3). ^{13}C NMR (100 MHz; $CDCl_3$; Me_4Si): 153.91; 141.80; 137.92; 132.00; 130.49; 129.47; 127.96; 126.71; 122.73; 117.21; 74.94; 31.90; 30.41; 29.50; 29.35; 26.12; 22.72; 14.14. Anal. calcd for: $C_{36}H_{42}Br_2N_2O_2$: C, 62.26; H, 6.10; N, 4.03; O, 4.61 found: C, 60.16; H, 5.78; N, 3.79; O, 5.11%.

11,12-Bis(octyloxy)-10,13-di(thiophen-2-yl)dibenzo[*a*,*c*]phenazine

10,13-Dibromo-11,12-bis(octyloxy)dibenzo[*a*,*c*]phenazine (1.0 g, 1.44 mmol) and trimethyl(thiophen-2-yl)stannane (1.35 ml, 4.3 mmol) in toluene (37 ml) were added to $PdCl_2(PPh_3)_2$ (0.101 g, 0.15 mmol) under a nitrogen atmosphere. After refluxing for 48 hours at 80 °C, the mixture was cooled to room temperature and then poured into H_2O; the organic layer was extracted with $CHCl_3$ and dried over anhydrous Na_2SO_4. The crude product was purified by column chromatography on silica gel to obtain the product as an orange liquid (0.6 g, 59.3%). ^{1}H NMR (400 MHz; $CDCl_3$; Me_4Si): 9.11 (d, 2H; Ar) 8.30 (t, 2H; Ar) 7.98 (t, 2H; Ar) 7.58(d, 2H; Ar) 7.53(m, 4H; Ar) 7.20(t, 2H; Ar) 3.98(t, 4H; CH_2) 1.72(m, 4H; CH_2) 1.34(m, 4H; CH_2) 1.21(m, 16H; CH_2) 0.82(t, 6H; CH_3). ^{13}C NMR (100 MHz; $CDCl_3$; Me_4Si): 153.10; 140.34; 138.02; 133.71; 131.89; 130.93; 130.44; 129.71; 127.85; 127.77; 127.10; 126.08; 124.26; 122.67; 74.21; 31.93; 30.51; 29.56; 29.37; 26.14; 22.76; 14.21.

10,13-Bis(5-bromothiophen-2-yl)-11,12-bis(octyloxy)dibenzo[*a*,*c*]phenazine (M4)

Under a nitrogen atmosphere, 11,12-bis(octyloxy)-10,13-di(thiophen-2-yl)dibenzo[*a*,*c*]phenazine (0.3 g, 0.427 mmol) was dissolved in 30 ml of THF, and NBS (0.174 g, 0.982 mmol) was then added in portions. The mixture was stirred for 24 h at room temperature. Then, the mixture was poured into water and extracted with chloroform. The combined organic layers were dried over Na_2SO_4, and then the solvent was removed. The crude product was purified by column chromatography to obtain **M2** as a red liquid (0.24 g, 65.4%). ^{1}H NMR (400 MHz; $CDCl_3$; Me_4Si): 9.10 (d, 2H; Ar) 8.31 (t, 2H; Ar) 7.90 (t, 2H; Ar) 7.60(d, 4H; Ar) 7.20(m, 2H; Ar) 3.98(t, 4H; CH_2) 1.72(m, 4H; CH_2) 1.34(m, 4H; CH_2) 1.21(m, 16H; CH_2) 0.82(t, 6H; CH_3) ^{13}C NMR (100 MHz; $CDCl_3$; Me_4Si): 152.75; 140.39; 137.18; 135.21; 131.88; 131.26; 130.03; 029.87; 128.94; 127.83; 127.14; 123.29; 122.62; 115.74; 74.23; 31.91; 30.54; 29.73; 29.55; 29.37; 26.15; 22.75; 14.18.

Poly[quinacridone-*alt*-(octyloxy)quinoxaline] (PQCQx)

5,8-Bis(5-bromothiophen-2-yl)-6,7-bis(octyloxy)quinoxaline (**M2**) (0.22 g, 0.31 mmol), 2,9-diboronic ester-*N*,*N*′-di(2-octyl-dodecyl) quinacridone (**M1**) (0.35 g, 0.31 mmol), $Pd(PPh_3)_4(0)$ (0.010 g, 0.009 mmol) and Aliquat 336 were placed in a Schlenk tube, purged with three nitrogen/vacuum cycles, and under a nitrogen atmosphere added 2 M degassed aqueous K_2CO_3 (10 ml) and dry toluene (20 ml). The mixture was heated to 90 °C and stirred in the dark for 24 h. After the polymerization was

over, the polymer was end-capped with bromothiophene. After reaction quenching, the whole mixture was poured into methanol. The precipitate was filtered off and purified by Soxhlet extraction with solvents in the order methanol, acetone and chloroform. The polymer was recovered from the chloroform fraction and precipitated into methanol. The final product was obtained as a dark red solid after drying in vacuum (0.33 g, 74%). Anal. calcd for: $C_{92}H_{132}N_4O_4S_2$: C, 77.70; H, 9.36; N, 3.94; O, 4.50; S, 4.51 found: C, 76.74; H, 9.25; N, 3.74; O, 5.31; S, 5.31%.

Poly[quinacridone-*alt*-(octyloxy)diphenylquinoxaline] (PQCTQx)

5,8-Bis(5-bromothiophen-2-yl)-6,7-bis(octyloxy)-2,3-diphenylquinoxaline (**M3**) (0.23 g, 0.27 mmol), 2,9-diboronic ester-*N*,*N*′-di(2-octyl-dodecyl)quinacridone (**M1**) (0.30 g, 0.27 mmol), $Pd(PPh_3)_4$-(0) (0.009 g, 0.008 mmol) and Aliquat 336 were placed in a Schlenk tube, purged with three nitrogen/vacuum cycles, and under a nitrogen atmosphere added 2 M degassed aqueous K_2CO_3 (10 ml) and dry toluene (20 ml). The mixture was heated to 90 °C and stirred in the dark for 24 h. After the polymerization was over, the polymer was end-capped with bromothiophene. After reaction quenching, the whole mixture was poured into methanol. The precipitate was filtered off and purified by Soxhlet extraction with solvents in the order methanol, acetone and chloroform. The polymer was recovered from the chloroform fraction and precipitated into methanol. The final product was obtained as a dark violet solid after drying in vacuum (0.37 g, 85%). Anal. calcd for: $C_{104}H_{140}N_4O_4S_2$: C, 79.34; H, 8.96; N, 3.56; O, 4.06; S, 4.07 found: C, 79.24; H, 8.20; N, 3.56; O, 4.96; S, 3.91%.

Poly[quinacridone-*alt*-(octyloxy)dibenzophenazine] (PQCTPz)

10,13-Bis(5-bromothiophen-2-yl)-11,12-bis(octyloxy)dibenzo[*a*,*c*]-phenazine (**M4**) (0.23 g, 0.27 mmol), 2,9-diboronic ester-*N*,*N*′-di(2-octyl-dodecyl)quinacridone (**M1**) (0.30 g, 0.27 mmol), $Pd(PPh_3)_4$(0) (0.009 g, 0.008 mmol) and Aliquat 336 were placed in a Schlenk tube, purged with three nitrogen/vacuum cycles, and under a nitrogen atmosphere added 2 M degassed aqueous K_2CO_3 (10 ml) and dry toluene (20 ml). The mixture was heated to 90 °C and stirred in the dark for 24 h. After the polymerization was over, the polymer was end-capped with bromothiophene. After reaction quenching, the whole mixture was poured into methanol. The precipitate was filtered off and purified by Soxhlet extraction with solvents in the order methanol, acetone and chloroform. The polymer was recovered from the chloroform fraction and precipitated into methanol. The final product was obtained as a dark violet solid after drying in vacuum (0.18 g, 40%). Anal. calcd for: $C_{104}H_{138}N_4O_4S_2$: C, 79.44; H, 8.85; N, 3.56; O, 4.07; S, 4.08 found: C, 78.91; H, 7.89; N, 3.60; O, 4.77; S, 4.23%.

Conclusions

In this study, a poly[quinacridone-*alt*-quinoxaline] series was successfully synthesized using the Suzuki coupling reaction by introducing a planar quinacridone unit and a highly soluble quinoxaline unit. The polymers had high molecular weights and good thermal stability. The ICT effects were much stronger in PQCTPz than in PQCQx and PQCTQx due to the structure of the phenyl ring. According to X-ray diffraction measurements, PQCQx and PQCTPz formed an ordered lamellar structure and displayed conventional edge-on π-stacking. In contrast, PQCTQx formed a face-on structure relative to the substrate. The open-circuit voltage (V_{OC}), short-circuit current (J_{SC}), fill factor (FF), and power conversion efficiency (PCE) of PQCTQx at a ratio of 1 : 2 with $PC_{71}BM$ were 0.83 V, 5.3 mA cm^{-2}, 51.1%, and 2.3%, respectively, due to its high molecular weight and face-on orientation compared with that of PQCQx and PQCTPz. For the device structure of ITO/PEDOT:PSS/active layer (PQCTQx:$PC_{71}BM$ = 1 : 2 with DIO)/PFN/Al, the values of V_{OC}, J_{SC}, FF and PCE were 0.85 V, 7.6 mA cm^{-2}, 54.9%, and 3.6%, respectively. Micro-phase separation occurred between the PQCTQx and $PC_{71}BM$, while the PQCTQx formed a small size domain at a 1 : 2 PQCTQx/$PC_{71}BM$ ratio. More effective performance levels could likely be obtained if the chemical and device structures of the polymer were optimized.

Acknowledgements

This research was supported by a grant from the Fundamental R&D Program for Core Technology of Materials funded by the Ministry of Knowledge Economy, Republic of Korea. This work was supported by the National Research Foundation of Korea Grant funded by the Korean Government (MEST) (NRF-2009-C1AAA001-2009-0093526).

Notes and references

1 R. H. Friend, R. W. Gymer, A. B. Holmes, J. H. Burroughes, R. N. Marks, C. Taliani, D. D. C. Bradley, D. A. D. Santos, J. L. Bredas, M. Logdlund and W. R. Salaneck, *Nature*, 1999, **397**, 121.
2 K. Zhang, Z. Chen, C. Yang, Y. Zou, S. Gong, Y. Tao, J. Qin and Y. Cao, *J. Mater. Chem.*, 2008, **18**, 3366.
3 H. J. Song, J. Y. Lee, I. S. Song, D. K. Moon and J. R. Haw, *J. Ind. Eng. Chem.*, 2011, **17**, 352.
4 X. Guo, C. Qin, Y. Cheng, Z. Xie, Y. Geng, X. Jing, F. Wang and L. Wang, *Adv. Mater.*, 2009, **21**, 3682.
5 S. Subramaniyan, H. Xin, F. S. Kim, S. Shoaee, J. R. Durrant and S. A. Jenekhe, *Adv. Energy Mater.*, 2011, **1**, 854.
6 J.-Y. Lee, S.-H. Kim, I.-S. Song and D.-K. Moon, *J. Mater. Chem.*, 2011, **21**, 16480.
7 Z.-G. Zhang and J. Wang, *J. Mater. Chem.*, 2012, **22**, 4178.
8 H. Yi, S. Al-Faifi, A. Iraqi, D. C. Watters, J. Kingsley and D. G. Lidzey, *J. Mater. Chem.*, 2011, **21**, 13649.
9 G. Li, V. Shrotriya, J. Huang, Y. Yao, T. Moriarty, K. Emery and Y. Yang, *Nat. Mater.*, 2005, **4**, 864.
10 Y. Zhu, R. D. Champion and S. A. Jenekhe, *Macromolecules*, 2006, **39**, 8712.
11 I. McCulloch, M. Heeney, C. Bailey, K. Genevicius, I. MacDonald, M. Shkunov, D. Sparrowe, S. Tierney,

R. Wagner, W. Zhang, M. L. Chabinyc, R. J. Kline, M. D. McGehee and M. F. Toney, *Nat. Mater.*, 2006, **5**, 328.

12 J. Mei, D. H. Kim, A. L. Ayzner, M. F. Toney and Z. Bao, *J. Am. Chem. Soc.*, 2011, **133**, 20130.

13 C.-J. Lin, W.-Y. Lee, C. Lu, H.-W. Lin and W.-C. Chen, *Macromolecules*, 2011, **44**, 9565.

14 J.-M. Jiang, P.-A. Yang, T.-H. Hsieh and K.-H. Wei, *Macromolecules*, 2011, **44**, 9155.

15 S. De Feyter, A. Gesquière, F. C. De Schryver, U. Keller and K. Müllen, *Chem. Mater.*, 2002, **14**, 989.

16 X. Yang, J. Wang, X. Zhang, Z. Wang and Y. Wang, *Langmuir*, 2007, **23**, 1287.

17 I. Osaka, M. Akita, T. Koganezawa and K. Takimiya, *Chem. Mater.*, 2012, **24**, 1235.

18 H.-J. Song, D.-H. Kim, E.-J. Lee, S.-W. Heo, J.-Y. Lee and D.-K. Moon, *Macromolecules*, 2012, **45**, 7815.

19 Y. Lee, Y. M. Nam and W. H. Jo, *J. Mater. Chem.*, 2011, **21**, 8583.

20 N. Blouin, A. Michaud, D. Gendron, S. Wakim, E. Blair, R. Neagu-Plesu, M. Belletête, G. Durocher, Y. Tao and M. Leclerc, *J. Am. Chem. Soc.*, 2008, **130**, 732.

21 R. Qin, W. Li, C. Li, C. Du, C. Veit, H.-F. Schleiermacher, M. Andersson, Z. Bo, Z. Liu, O. Inganäs, U. Wuerfel and F. Zhang, *J. Am. Chem. Soc.*, 2009, **131**, 14612.

22 S. K. Lee, W.-H. Lee, J. M. Cho, S. J. Park, J.-U. Park, W. S. Shin, J.-C. Lee, I.-N. Kang and S.-J. Moon, *Macromolecules*, 2011, **44**, 5994.

23 X. K. Gao, Y. Wang, X. D. Yang, Y. Q. Liu, W. F. Qiu, W. P. Wu, H. J. Zhang, T. Qi, Y. Liu, K. Lu, C. Y. Du, Z. G. Shuai, G. Yu and D. B. Zhu, *Adv. Mater.*, 2007, **19**, 3037.

24 I. Osaka, T. Abe, S. Shinamura, E. Miyazaki and K. Takimiya, *J. Am. Chem. Soc.*, 2010, **132**, 5000.

25 J. C. Bijleveld, A. P. Zoombelt, S. G. J. Mathijssen, M. M. Wienk, M. Turbiez, D. M. de Leeuw and R. A. J. Janssen, *J. Am. Chem. Soc.*, 2009, **131**, 16616.

26 A. Gadisa, W. Mammo, L. M. Andersson, S. Admassie, F. Zhang, M. R. Andersson and O. Inganäs, *Adv. Funct. Mater.*, 2007, **17**, 3836.

27 Z. He, C. Zhong, X. Huang, W.-Y. Wong, H. Wu, L. Chen, S. Su and Y. Cao, *Adv. Mater.*, 2011, **23**, 4636.

28 E. Wang, L. Hou, Z. Wang, Z. Ma, S. Hellström, W. Zhuang, F. Zhang, O. Inganäs and M. R. Andersson, *Macromolecules*, 2011, **44**, 2067.